Applied Physics Letters

Wave-canceling acoustic metarod architected with single material building blocks

Cite as: Appl. Phys. Lett. **116**, 241904 (2020); https://doi.org/10.1063/5.0011319
Submitted: 20 April 2020 . Accepted: 03 June 2020 . Published Online: 17 June 2020

Akira Ogasawara, Kentaro Fujita, Motonobu Tomoda, Osamu Matsuda, and Oliver B. Wright

Applied Physics Letters ARTICLE scitation.org/journal/apl

Wave-canceling acoustic metarod architected with single material building blocks

Cite as: Appl. Phys. Lett. **116**, 241904 (2020); doi: 10.1063/5.0011319
Submitted: 20 April 2020 · Accepted: 3 June 2020 ·
Published Online: 17 June 2020

Akira Ogasawara, Kentaro Fujita, Motonobu Tomoda, Osamu Matsuda, and Oliver B. Wright[a]

AFFILIATIONS

Division of Applied Physics, Graduate School of Engineering, Hokkaido University, Sapporo 060-8628, Japan

[a]Author to whom correspondence should be addressed: olly@eng.hokudai.ac.jp

ABSTRACT

Preventing elastic waves from traveling down thin structures is a subject of great interest from the point of view of both physics and applications. It represents a problem—mirrored by the case of light in waveguides—that has broad implications. To completely prohibit sound waves in a given frequency range in rods, for example, all axially propagating acoustic eigenmodes must exhibit strong damping. Here, we demonstrate experimentally and by simulation a metamaterial rod made from a single material that can simultaneously shut out all elastic-wave polarizations, namely longitudinal, flexural, and torsional modes, in a band in the sub-kHz range. We first bond five acrylic building blocks together to make a subwavelength resonator and then fix an array of these inside an acrylic tube to form a cylindrical metarod that inhibits sound transmission in the metamaterial bandgap frequency range. Applications include vibration control and earthquake mitigation.

Following on from the dawn of electromagnetic metamaterials,[1,2] their acoustic analogs,[3] based on subwavelength vibrational resonators, have shown great promise in a variety of applications, including superlensing,[4–6] negative refraction,[7,8] cloaking,[9–12] and damping.[13–31] In a practical sense, damping is by far the most important application of acoustic metamaterials, in particular, in the context of vibration control and preventing damage from earthquakes.

Being more elaborate in conception than in the electromagnetic case owing to the tensorial nature of elasticity, it is only recently that acoustic metamaterial rods or beams, i.e., metarods or metabeams, that block all sound polarizations have been proposed.[21,31] Ma *et al.* used a structure consisting of square cross section epoxy rods containing silicone-coated steel masses,[21] but did not experimentally demonstrate the existence of a perfect bandgap, i.e., for all eigenmodes. Fujita *et al.* used a complicated machined rectangular cross section aluminum beam to experimentally demonstrate a perfect bandgap in a single material,[31] but the high aspect ratio, ∼10 of their proposed metabeam is not suitable for the robust support of heavy objects.

There is a clear requirement for a simple metarod that is easy to fabricate, e.g., made of a single material, and that at the same time exhibits a perfect bandgap to block all acoustic eigenmodes. Perfect-bandgap phononic crystal beams or rods—exhibiting periodicities comparable to the acoustic wavelength[32–38]—have been demonstrated, but no single-material perfect-bandgap metamaterial rod has been proposed to date. If a metarod with such exotic properties was conceived and realized, with the potential for relatively large band gaps, it could clearly revolutionize the field of passive vibration control.

Here, we demonstrate by experiment and numerical simulation a perfect-bandgap acoustic metarod made of a single material, in this case consisting of bonded isotropic acrylic building blocks that form an overall circular cross section; we make use of a simple unit cell containing a cylindrical resonator supported on either side by cylindrical rods, all held in place by two compliant supports in an outer tube. By means of approximate analytical models, we tune the compressional, flexural, and torsional resonances of such a unit-cell array to form a triple-mode perfect bandgap in the sub-kHz region, forbidding the passage of all acoustic eigenmodes.

A 3D (three-dimensional) exploded view of the internal components of a unit cell of the proposed metarod, corresponding to the effective components after assembly, is shown in Fig. 1(a) in a vertical orientation. These building blocks, made of acrylic, consist of an inner cylinder, two shorter rods (labeled thin and thick), and two Y-shaped supports exhibiting threefold symmetry. Photographs of the machined components before assembly (except for the outer tube) and after assembly by dichloroethylene bonding are shown in Figs. 1(b) and 1(c), respectively. The assembly is facilitated by holes drilled in the two Y-shaped supports and in the inner cylinder. After assembly, the resonator consists of the inner cylinder, of length 38 mm and diameter

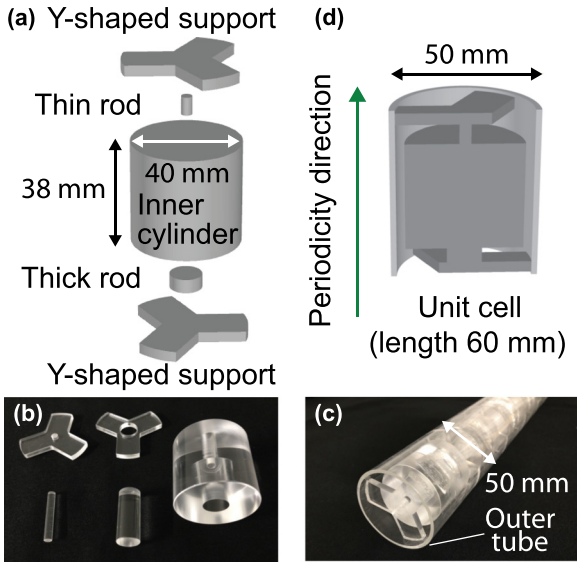

FIG. 1. Metarod design. (a) Exploded view of the internal components of the metarod, corresponding to the effective components after assembly by bonding. Each unit cell contains two Y-shaped supports, a thin rod, an inner cylinder, and a thick rod. (b) Photograph of the acrylic building blocks of the resonator before bonding. The outer tube is not shown. (c) Photograph of part of an assembled metarod of 10 unit cells. (d) Cross section of a unit cell. All dimensions are given in the supplementary material.

40 mm, connected to a thin rod of diameter 4 mm and length 6.7 mm, and a thick rod of diameter 12 mm and length 5.3 mm. Setting a difference between the thin and thick rod dimensions allows more degrees of freedom in tuning the resonant frequencies of the three acoustic eigenmodes, crucial to obtain a perfect bandgap. The design of the Y-supports of thickness 4 mm and diameter 46 mm allows them to act as springs for axial motion after bonding to the inner structure and outer tube. The spacing of two adjacent Y-supports is 2 mm, leading to a total unit-cell length of 60 mm, as shown by the cross section in Fig. 1(d). The assembly of the bonded resonators inside a length of outer tube of external diameter 50 mm and wall thickness 2 mm to make a 10-unit-cell structure is described in more detail in the supplementary material.

In designing the unit cell, our strategy is to set the lowest resonance for each of the three acoustic polarizations to roughly the same frequency in order to open a perfect bandgap. The roles of the rods and supports in the proposed geometry are different for each polarization, as described below. We first present numerical simulations of the chosen design, optimized to give a significant perfect bandgap, and then experimental results and simulations for sound transmission in a 10-unit-cell rod.

The approximate roles of the springs and masses in our meta-atom unit cell for each of the three polarizations are shown in Figs. 2(a), 2(d), and 2(g), which can be better understood by reference to the on-resonance results of finite element numerical simulations with COMSOL Multiphysics (version 5.4) for a single unit cell with two fixed boundaries perpendicular to the axial direction. We show kinetic- and strain-energy density plots in Figs. 2(b), 2(e), 2(h) and 2(c), 2(f), 2(i), respectively, also viewable as an animation (Multimedia

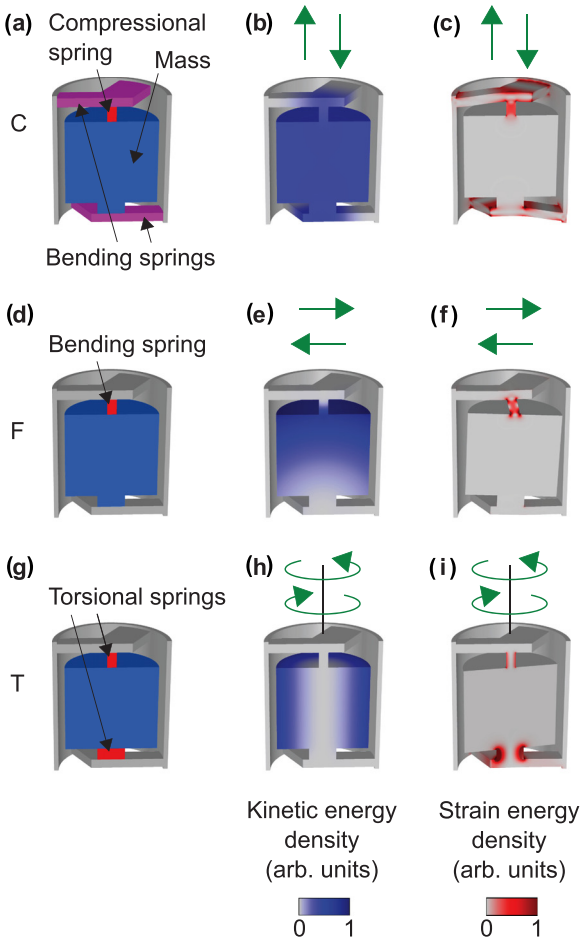

FIG. 2. Analytical interpretation of the metarod geometry using masses and springs, and simulated single-cell acoustic eigenmodes with rigid boundary conditions. (a) For the compressional resonance (C, motion along the axial direction). Red and magenta regions act as springs. Blue and gray regions act as masses and rigid frames, respectively. (b) and (c) Simulated kinetic and strain energy density distributions, respectively, for the compressional eigenmode. Green arrows show dominant displacement directions. (d)–(i) Similar figures for the flexural (F, motion perpendicular to the axial direction) and torsional (T, rotation about the central axis) resonances. Multimedia View: https://doi.org/10.1063/5.0011319.1.

View). The kinetic energy plots serve to highlight in blue the structures that act as effective resonator masses, whereas the potential energy plots serve to highlight in red the structures that act as effective springs. The compressional, flexural, and torsional resonance frequencies, 808, 795, and 743 Hz, are all tuned close to 800 Hz by iterative simulation of the dimensions of the inner cylinder, rods, and Y-supports while examining the acoustic dispersion relation for a perfect bandgap, as described below. The density and the longitudinal and transverse sound velocities of the metarod are taken as $\rho = 1190\,\mathrm{kg\,m^{-3}}$, $v_l = 2077\ \mathrm{m\,s^{-1}}$, and $v_t = 998\ \mathrm{m\,s^{-1}}$, respectively, and internal friction is ignored.[39] As shown by the green arrows, for the compressional resonance (C), the inner cylinder vibrates along the axial direction, for the flexural resonance (F) it swings along the width direction, and for the torsional resonance (T) it rotates about the

central axis. In this way, a triple-mode resonant structure is created. Because of the rotational symmetry,[40] the +120° and −120° axial rotations of the flexural eigenmode shown in Figs. 2(e) and 2(f) appear to represent three degenerate eigenmodes, but in fact there are only two because the third one can expressed as a linear combination of the other two.

It is useful to derive the dependence of each resonant frequency on the chosen geometrical parameters by means of simple approximate analytical models. This is done in the supplementary material, giving reasonable agreement with the simulations.

The numerically derived dispersion relation using periodic boundary conditions is shown in Fig. 3, revealing the existence of a perfect bandgap from 720 to 980 Hz arising from local resonances, where the band gaps for the three types of eigenmode overlap. Although the rod can guide three distinct acoustic polarizations, this structure damps out all axially propagating acoustic eigenmodes in the bandgap region. The similarity of the dispersion of the C and T modes below the bandgap is coincidental. Owing to the elastic coupling of the outer cylinder with the internal structure, the respective low frequency sound velocities 810 and 690 ms^{-1} for these two modes are significantly smaller than either that for torsional modes ($v_t = 998$ ms^{-1}) or compressional modes ($\lesssim v_l = 2077$ ms^{-1}) in the outer cylinder alone.[41]

We measure the sound transmission for all three eigenmodes by means of a 10-unit-cell metarod of length 600 mm, connected on either side to an extra portion of bare tube of length 4 mm beyond the unit cells (giving two 5 mm gaps from the Y-support outer surfaces to the ends of the outer tube). The experiment for the compressional eigenmode is briefly described here, the remaining details being

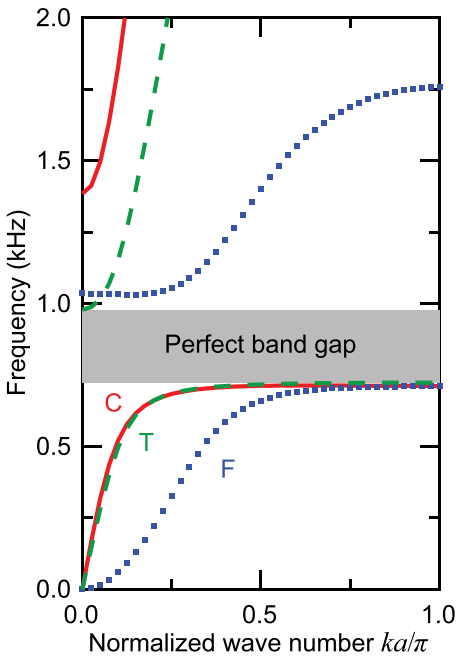

FIG. 3. Acoustic dispersion relation for axial propagation in the metarod; *k* and *a* are the axial wavevector and unit-cell length, respectively. The solid red, dotted blue, and dashed green curves correspond to compressional (C), flexural (F), and torsional (T) eigenmodes, respectively. Branches of the two degenerate flexural eigenmodes overlap.

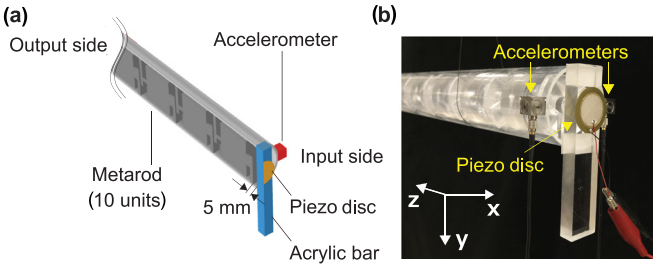

FIG. 4. Experimental setup for compressional-eigenmode transmission. (a) Schematic diagram of the setup. A portion along the length in cross section is shown. The outer tube, inner resonators, piezo disk, acrylic bar for sound excitation, and accelerometer are shown by the light gray region, dark gray region, orange semicircle, blue bar, and red cube, respectively. (b) Photograph showing the compressional eigenmode excitation setup at the input end of the rod. The output end, that also includes two accelerometers, is not shown.

reserved for the supplementary material. The apparatus is shown in Fig. 4. The sample, horizontally suspended by fishing lines, is excited by a sinusoidally driven piezoelectric disk (Murata Manufacturing 7BB-41–2L0) bonded to an acrylic bar fixed in an asymmetric position on one end of the metarod (to also allow the excitation of flexural and torsional modes with appropriate piezo-disk attachment). Three-axis

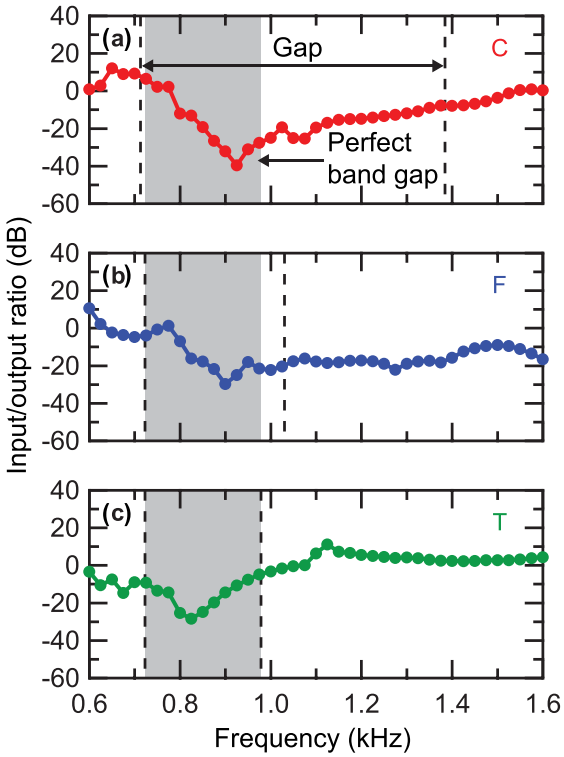

FIG. 5. Experimentally observed output/input ratio for each acoustic eigenmode for a finite metarod of 10 unit cells plotted as a function of frequency on a logarithmic scale. (a)–(c) correspond to the compressional, flexural and torsional eigenmodes, respectively. The vertical dashed lines indicate the band gaps for each eigenmode expected from the simulations, whereas the gray shaded region in each case corresponds to the perfect bandgap expected from the simulations.

accelerometers (Fuji Ceramics SA12ZSCA) are used at two points at both ends of the metarod [see the red cube in Fig. 4(a) and yellow arrows in (b) for the position of their placement at the input end in experiment] together with lock-in detection, in order to obtain a measure of the acoustic wave damping.

The measured spectra for the output/input ratio for all three eigenmodes are shown on a logarithmic scale in Fig. 5 together with the band gaps found by simulation. Outside the bandgap regions, interference by multiple acoustic reflections is expected to occur, producing local maxima and minima, but all modes show marked damping in the bandgap region. It is difficult to precisely determine the perfect bandgap experimentally, but the output/input intensity ratio for all modes takes a value less than 0.25 (−6 dB) between 800 and 980 kHz. This relatively broad band, making up ∼20% of the midgap frequency in reasonable correspondence with the simulations, demonstrates a perfect-bandgap behavior unprecedented in experiments on metarods. Our results can also be expressed in terms of effective decay lengths, as detailed in the supplementary material. For example, at ∼850 Hz, the typical experimental decay constant, ∼5 m^{-1} for all modes, implies that sound propagation through 10 unit cells is sufficient to almost completely damp out the acoustic amplitude by a factor of ∼20. This factor is smaller than that predicted by the simulations (see the supplementary material). We attribute this difference, as well as some observed differences in the band edges, to imperfections in fabrication, such as the neglect of the effect of the bonding agent or air bubbles in the bonds, or to residual sound transmitted through the air.

In order to investigate the effect of the outer geometry on the dispersion relation and unit-cell resonant frequencies, we separately vary by simulation the adjacent Y-support separation $2t_r$ that governs the lattice constant, and the outer tube thickness t_p (see Fig. S1 of the supplementary material). Figure 6 shows the resulting variation of the band gaps and single-cell resonances on varying t_r and t_p in the ranges 1 ± 0.75 mm and 2 ± 1.5 mm, respectively, away from their design values. Monotonic changes in the bandgap widths are seen only for variations in the tube thickness t_p, as expected from our assumption that the structure is behaving as a metamaterial dependent on the local resonances rather than as a phononic crystal dependent on the lattice constant. The bandgap narrowing with t_p shows that the outer tube rigidity also plays some role in determining the band edges, presumably because the relatively long unit-cell length involves a non-negligible compliance. However, only the compressional mode unit-cell resonant frequency depends significantly on t_p. The dimensions of our chosen structure are optimized for the commercially available outer-tube thickness $t_p = 2$ mm. On the theoretical side, it would be interesting to derive the effective parameters of the metarod for particular modes by means of a homogenization scheme, although this is beyond the scope of the present paper.[42] This would allow a better understanding of the presence or lack of impedance matching between this structure and others.

In conclusion, we have demonstrated in experiment and by simulation that a metarod architecture consisting of acrylic building blocks in the form of a periodic triple-mode resonator array displays a perfect acoustic bandgap. In the bandgap region, just below 1 kHz, the metarod efficiently damps out compressional, flexural, and torsional vibrations. Larger stop bands should be accessible by the use of graded metarods, unlocking more avenues for practical use. Also, because the building blocks of this robust structure can also be 3D printed or cast, lower or higher frequencies may be conveniently accessed by the use

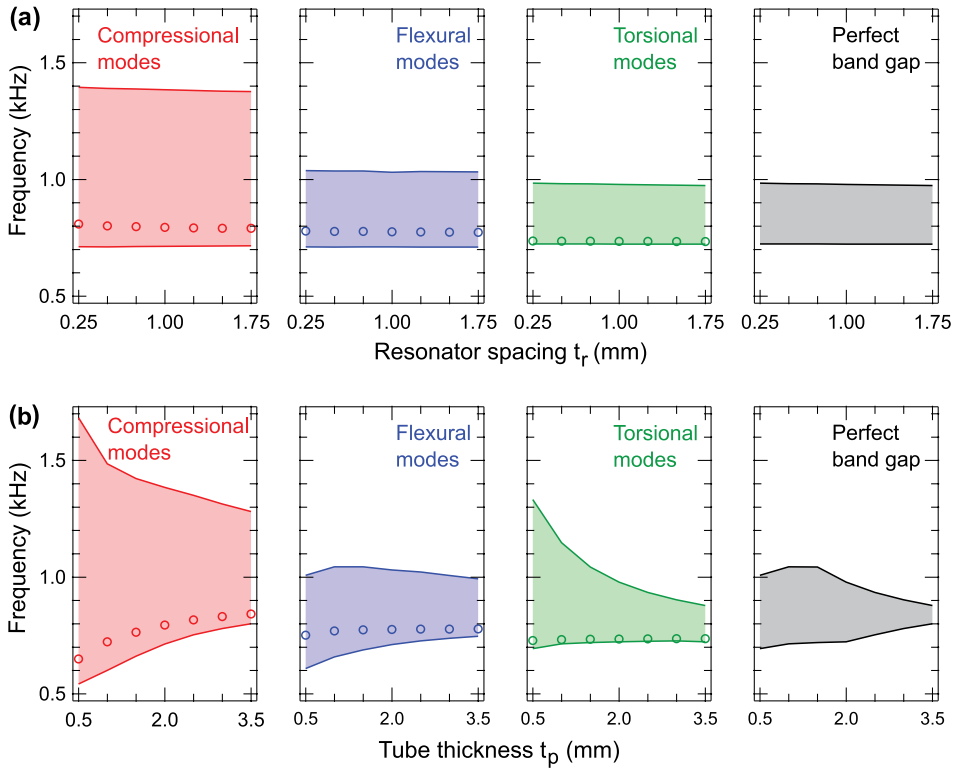

FIG. 6. Simulated bandgap variation and unit-cell eigenmode frequencies on varying the length t_r, where the adjacent Y-support separation is $2t_r$, and the outer tube thickness t_p. (a) and (b) indicate the effect of separately varying t_r and t_p, respectively, from their design values of 1 mm and 2 mm. The solid lines correspond to the top and bottom frequencies of each bandgap and the perfect bandgap. The colored areas indicate the gap regions. The open circles show eigenmode frequencies calculated for a single unit cell.

of softer materials such as rubber or harder materials such as steel or concrete, which should open the way to a host of applications not only in the damping of vibrations in industrial situations, but also in vehicles, ships, and aircraft. Moreover, scaling up the presented ideas to larger sizes should have important ramifications in the vibration isolation of buildings and in earthquake mitigation.

See the supplementary material for the approximate analytical models used to describe the metarod unit-cell resonant frequencies, the effective acoustic amplitude decay constants, and the details of the materials and methods. On-resonance animations of the unit-cell kinetic- and strain-energy densities are also included (Multimedia View).

We acknowledge Grants-in-Aid for Scientific Research from the Ministry of Education, Culture, Sports, Science and Technology (MEXT).

DATA AVAILABILITY

The data that support the findings of this study are available from the corresponding author upon reasonable request.

REFERENCES

[1]J. B. Pendry, A. J. Holden, D. J. Robbins, and W. Stewart, "Magnetism from conductors and enhanced nonlinear phenomena," IEEE Trans. Microwave Theory Tech. **47**, 2075–2084 (1999).
[2]R. A. Shelby, D. R. Smith, and S. Schultz, "Experimental verification of a negative index of refraction," Science **292**, 77–79 (2001).
[3]Z. Liu, X. Zhang, Y. Mao, Y. Zhu, Z. Yang, C. T. Chan, and P. Sheng, "Locally resonant sonic materials," Science **289**, 1734–1736 (2000).
[4]S. Zhang, L. Yin, and N. Fang, "Focusing ultrasound with an acoustic metamaterial network," Phys. Rev. Lett. **102**, 194301 (2009).
[5]L. Zigoneanu, B.-I. Popa, and S. A. Cummer, "Design and measurements of a broadband two-dimensional acoustic lens," Phys. Rev. B **84**, 024305 (2011).
[6]F. Lemoult, N. Kaina, M. Fink, and G. Lerosey, "Soda cans metamaterial: A subwavelength-scaled phononic crystal," Crystals **6**, 82 (2016).
[7]V. M. García-Chocano, J. Christensen, and J. Sánchez-Dehesa, "Negative refraction and energy funneling by hyperbolic materials: An experimental demonstration in acoustics," Phys. Rev. Lett. **112**, 144301 (2014).
[8]R. Zhu, X. Liu, G. Hu, C. Sun, and G. Huang, "Negative refraction of elastic waves at the deep-subwavelength scale in a single-phase metamaterial," Nat. Commun. **5**, 5510 (2014).
[9]J. Pendry and J. Li, "An acoustic metafluid: Realizing a broadband acoustic cloak," New J. Phys. **10**, 115032 (2008).
[10]A. N. Norris, "Acoustic metafluids," J. Acoust. Soc. Am. **125**, 839–849 (2009).
[11]N. Stenger, M. Wilhelm, and M. Wegener, "Experiments on elastic cloaking in thin plates," Phys. Rev. Lett. **108**, 014301 (2012).
[12]T. Bückmann, M. Thiel, M. Kadic, R. Schittny, and M. Wegener, "An elasto-mechanical unfeelability cloak made of pentamode metamaterials," Nat. Commun. **5**, 4130 (2014).
[13]N. Fang, D. Xi, J. Xu, M. Ambati, W. Srituravanich, C. Sun, and X. Zhang, "Ultrasonic metamaterials with negative modulus," Nat. Mater. **5**, 452 (2006).
[14]D. Yu, Y. Liu, G. Wang, H. Zhao, and J. Qiu, "Flexural vibration band gaps in Timoshenko beams with locally resonant structures," J. Appl. Phys. **100**, 124901 (2006).
[15]S. Yao, X. Zhou, and G. Hu, "Experimental study on negative effective mass in a 1D mass–spring system," New J. Phys. **10**, 043020 (2008).
[16]Y. Xiao, J. Wen, D. Yu, and X. Wen, "Flexural wave propagation in beams with periodically attached vibration absorbers: Band-gap behavior and band formation mechanisms," J. Sound Vib. **332**, 867–893 (2013).
[17]S. Zhang, J. Hui Wu, and Z. Hu, "Low-frequency locally resonant band-gaps in phononic crystal plates with periodic spiral resonators," J. Appl. Phys. **113**, 163511 (2013).
[18]R. Zhu, X. Liu, G. Hu, C. Sun, and G. Huang, "A chiral elastic metamaterial beam for broadband vibration suppression," J. Sound Vib. **333**, 2759–2773 (2014).
[19]M. Nouh, O. Aldraihem, and A. Baz, "Vibration characteristics of metamaterial beams with periodic local resonances," J. Vib. Acoust. **136**, 061012 (2014).
[20]H. Zhang, Y. Xiao, J. Wen, D. Yu, and X. Wen, "Flexural wave band gaps in metamaterial beams with membrane-type resonators: Theory and experiment," J. Phys. D **48**, 435305 (2015).
[21]G. Ma, C. Fu, G. Wang, P. Del Hougne, J. Christensen, Y. Lai, and P. Sheng, "Polarization bandgaps and fluid-like elasticity in fully solid elastic metamaterials," Nat Commun. **7**, 13536 (2016).
[22]T. Wang, M.-P. Sheng, and Q.-H. Qin, "Multi-flexural band gaps in an Euler–Bernoulli beam with lateral local resonators," Phys. Lett. A **380**, 525–529 (2016).
[23]L. Li and A. Cai, "Low-frequency band gap mechanism of torsional vibration of lightweight elastic metamaterial shafts," Eur. Phys. J. Appl. Phys. **75**, 10501 (2016).
[24]E. Nobrega, F. Gautier, A. Pelat, and J. Dos Santos, "Vibration band gaps for elastic metamaterial rods using wave finite element method," Mech. Syst. Signal Process. **79**, 192–202 (2016).
[25]L. Tang and L. Cheng, "Ultrawide band gaps in beams with double-leaf acoustic black hole indentations," J. Acoust. Soc. Am. **142**, 2802–2807 (2017).
[26]H. Chen, X. Li, Y. Chen, and G. Huang, "Wave propagation and absorption of sandwich beams containing interior dissipative multi-resonators," Ultrasonics **76**, 99–108 (2017).
[27]J.-S. Chen, Y.-J. Huang, and I.-T. Chien, "Flexural wave propagation in metamaterial beams containing membrane-mass structures," Int. J. Mech. Sci. **131–132**, 500–506 (2017).
[28]L. Li, R. Lv, A. Cai, M. Xie, Y. Chen, and G. Huang, "Low-frequency vibration suppression of a multi-layered elastic metamaterial shaft with discretized scatters," J. Phys. D **52**, 055105 (2019).
[29]K. Wang, J. Zhou, D. Xu, and H. Ouyang, "Tunable low-frequency torsional-wave band gaps in a meta-shaft," J. Phys. D **52**, 055104 (2019).
[30]K. Wang, J. Zhou, Q. Wang, H. Ouyang, and D. Xu, "Low-frequency band gaps in a metamaterial rod by negative-stiffness mechanisms: Design and experimental validation," Appl. Phys. Lett. **114**, 251902 (2019).
[31]K. Fujita, M. Tomoda, O. B. Wright, and O. Matsuda, "Perfect acoustic bandgap metabeam based on a quadruple-mode resonator array," Appl. Phys. Lett. **115**, 081905 (2019).
[32]F.-C. Hsu, C.-I. Lee, J.-C. Hsu, T.-C. Huang, C.-H. Wang, and P. Chang, "Acoustic band gaps in phononic crystal strip waveguides," Appl. Phys. Lett. **96**, 051902 (2010).
[33]Y. Pennec, B. D. Rouhani, C. Li, J. Escalante, A. Martínez, S. Benchabane, V. Laude, and N. Papanikolaou, "Band gaps and cavity modes in dual phononic and photonic strip waveguides," AIP Adv. **1**, 041901 (2011).
[34]S. Mizuno, "Acoustic phonon modes and phononic bandgaps in GaN/AlN nanowire superlattices," Nanoscale Res. Lett. **7**, 479 (2012).
[35]F.-C. Hsu, J.-C. Hsu, T.-C. Huang, C.-H. Wang, and P. Chang, "Reducing support loss in micromechanical ring resonators using phononic band-gap structures," J. Phys. D **44**, 375101 (2011).
[36]D. Feng, D. Xu, G. Wu, B. Xiong, and Y. Wang, "Extending of band gaps in silicon based one-dimensional phononic crystal strips," Appl. Phys. Lett. **103**, 151906 (2013).
[37]D. Feng, D. Xu, G. Wu, B. Xiong, and Y. Wang, "Phononic crystal strip based anchors for reducing anchor loss of micromechanical resonators," J. Appl. Phys. **115**, 024503 (2014).
[38]S. Jiang, H. Hu, and V. Laude, "Low-frequency band gap in cross-like holey phononic crystal strip," J. Phys. D **51**, 045601 (2018).
[39]See https://www.m-chemical.co.jp/acrylite/information/ for the COMSOL library (in Japanese).
[40]K. Nagaya, "Dispersion of elastic waves in bars with polygonal cross section," J. Acoust. Soc. Am. **70**, 763–770 (1981).
[41]J. L. Rose, *Ultrasonic Waves in Solid Media* (Dover, 2000).
[42]M. Yang, G. Ma, Y. Wu, Z. Yang, and P. Sheng, "Homogenization scheme for acoustic metamaterials," Phys. Rev. B **89**, 064309 (2014).